Proceedings Paper:
McCullough, D.R., Jones, B., Villarreal, O.J.G. et al. (1 more author) (2021) Towards control of autonomous surface vehicles in rough seas. In: Findeisen, R., Hirche, S., Janschek, K. and Mönnigmann, M., (eds.) IFAC-PapersOnLine. 21st IFAC World Congress 2020, 11-17 Jul 2020, Berlin, Germany. International Federation of Automatic Control (IFAC) , pp. 14692-14697.

https://doi.org/10.1016/j.ifacol.2020.12.1832

Available online at www.sciencedirect.com

ScienceDirect

IFAC PapersOnline CONFERENCE PAPER ARCHIVE

IFAC PapersOnLine 53-2 (2020) 14692–14697

Towards Control of Autonomous Surface Vehicles in Rough Seas

Daniel R. McCullough * **Bryn L. Jones** *
Oscar J.G. Villarreal * **J.A. Rossiter** *

* *Department of Automatic Control and Systems Engineering, University of Sheffield, Sheffield United Kingdom.*

Abstract: This paper addresses the problem of controlling an Autonomous Surface Vehicle (ASV) in rough sea-states, with a view towards minimising wave-induced forces, whilst maintaining headway. This is a challenging control application since, and as is derived in the paper, the interaction between the vessel and the wave disturbance is nonlinear and coupled. This subsequently motivates the novel application of the Real Time Iteration Scheme (RTI) for Nonlinear Model Predictive Control (NMPC) of the ASV. Analysis of the resulting control signal provides an important insight into the role of the wave encounter frequency. Specifically, by actuating at twice the average wave encounter frequency, the nonlinear controller is able to reduce the wave forces, compared to an open-loop controller that achieves the same average velocity.

Keywords: Nonlinear and optimal marine system control, autonomous surface vehicle, nonlinear model predictive control, real time optimization.

1. INTRODUCTION

With the potential to replace manned vessels for dirty operations such as cleaning up oil spills, (Kim et al., 2012), dangerous ones, like those found in mine sweeping, or dull monotonous tasks like patrolling, (Oleynikova et al., 2010), the need for autonomous surface vehicles is increasing. This growth in use necessitates an increase in the ability of the Autonomous Surface Vehicle (ASV) to handle more extreme ocean environments, such as rough seas, in a similar or superior manner as human pilots.

Traditional path following controllers may neglect ocean disturbances, (Lekkas and Fossen, 2014; Oh and Sun, 2010; Çimen and Banks, 2004), or consider only ocean drift forces, (Paliotta et al., 2019; Peymani and Fossen, 2013). Larger vessels, such as container ships can often assume ocean disturbances to be planar for most conditions in sea state 3 or below on the Douglas Scale. For larger vessels in the presence of waves, constraining roll is important for reducing sea-sickness and damage to cargo (Li et al., 2009, 2010).

However, smaller sea going vessels of the magnitude of tens of meters or smaller are greatly impacted by waves. Reinhart et al. (2010) use a priori optimized control path templates to find that tacking in littoral waves reduces bow diving. This behavior is used in a path planning algorithm which, when the angle between desired direction of travel and the main wave direction is smaller than a predefined threshold a secondary point is added to the path to increase the angle and to create this tacking behaviour. A PID controller is used to maintain the planned path without knowledge of the ocean environment which reduces the bow diving but does not eliminate it. With a set maximum pitch and roll constraint, Ono et al. (2014), calculates feasible safe velocity regions for use in path planning in rough seas. The model used a direct input, that is the input is the velocity of the system, allowing it to move from one safe velocity region to the next in one time step. On a boat this would not be possible, and the boat would have to move through unsafe velocity regions and potentially capsize or bow dive. Therefore, in this work we propose an optimal control strategy that is based upon a first-principles model of the ASV and wave interaction dynamics, with a view towards minimising wave induced forces whilst maintaining headway.

The rest of the paper is organized as follows; section 2 presents the derivation of a low-order state space model that describes the coupled dynamics between the ASV and a wave, section 3 introduces the control problem formulation, section 4 presents the results and discussion from the simulations, and section 5 concludes the paper, and discusses future work.

2. SYSTEM MODEL

2.1 ASV Dynamics

The ASV model is based upon a simplified description of the Halcyon ASV: more details of the 6 degrees of freedom (DOF) model can be found in (Heins et al., 2017). For the purpose of developing initial control strategies this paper examines the 1 DOF scenario, with the changes and simplifications from the full model noted below. The simplification is based upon the following assumptions.

- The model degrees of freedom are restricted to forwards (surge) motion only. The state space model developed in this paper can be augmented with addi-

10.1016/j.ifacol.2020.12.1832

tional states to describe the other degrees of freedom and will be studied in future work.
- There are no water-current or wind-induced forces. Again, these can be included in the model but the focus of the present work is upon wave-induced forces.
- Actuation is restricted to the propeller input only. Future work will include steering once roll and yaw dynamics are included.
- The wave induced forces arise from a single wave harmonic, corresponding to regular waves, and the controller has full information of this. In practice, the sea surface is more complex and wave forecasting is an active research area (see: Merigaud and Ringwood (2019))
- The vessel is heading directly into the oncoming waves. This assumption will be relaxed in future work when steering inputs are considered.

The equations of motion of the boat in the surge direction are as follows:

$$\dot{\chi}(t) = \nu(t), \tag{1a}$$

$$\dot{\nu}(t) = \frac{D(\nu(t)) + \tau_{\mathrm{p}}(\nu(t), \zeta(t)) + \tau_{\mathrm{w}}^{\nu}(\nu(t), \eta(t))}{M}, \tag{1b}$$

$$\dot{\zeta}(t) = \frac{-1}{\kappa}\zeta(t) + \frac{1}{\kappa}u(t). \tag{1c}$$

The system has five states, $x = [\chi, \nu, \zeta, \eta, \dot{\eta}]^T$, with $\chi(t)$ being the position in the boat reference frame at time t, $\nu(t)$ is the surge velocity of the boat, $\zeta(t)$ is the propeller speed, $u(t)$ is the propeller control input, and $\eta(t)$ and $\dot{\eta}$ are wave states defined in the following section. In the above equations $D(\nu(t))$ is the drag term, $\tau_{\mathrm{p}}(\nu(t), \zeta(t))$ is the propulsion from the propellers, κ is the propellor time constant, and $\tau_{\mathrm{w}}^{\nu}(\nu(t), \eta(t))$ is the wave force in the surge direction, derived in the next section. Table A.1 in the appendix list the parameters employed in this paper. The surge drag force equation is as follows:

$$D(\nu(t)) = -\frac{1}{2}\rho S C_f^*(\nu(t))\nu(t)^2, \tag{2}$$

where S is the wetted hull surface area and ρ is the density of water. The modified resistance curve, $C_f^*(\nu(t))$,is approximated by the following 6th order polynomial:

$$D(\nu(t)) = -\frac{1}{2}\rho S(p_1\nu(t)^6 + p_2\nu(t)^5 + p_3\nu(t)^4 + p_4\nu(t)^3 + p_5\nu(t)^2 + p_6\nu(t) + p_7)\nu(t)^2, \tag{3}$$

where p_x are constant coefficients defined in appendix A.2. The thrust from the dual propellers is modelled by:

$$\tau_{\mathrm{p}}(\nu(t), \zeta(t)) = 2K_\tau \rho d^4 \zeta(t)^2, \tag{4}$$

where d is the propeller diameter and where the thrust parameter K_τ is given by:

$$K_\tau(J) = K_\tau^{\{1\}}J^2 + K_\tau^{\{2\}}J + K_\tau^{\{3\}}, \tag{5}$$

where, $K_\tau^{\{i\}}$ are thrust polynomial constants defined in appendix A.3, and the advance ratio, J, is:

$$J = \frac{\nu(t)}{\zeta(t)d}. \tag{6}$$

2.2 Wave Environment and Forces

The force exerted on the boat by the wave is calculated using a Response Amplitude Operator (RAO) (Fossen, 2011). The full model uses look-up tables to find the values dependent on the conditions. In the case of the surge direction, the force RAO is appoximately an affine function of the surge velocity and wave frequency, as shown in Figure 1. The phase RAO is assumed to be constant for all boat velocities at a specific wave frequency. For the force RAO, the force is linearly dependent on the velocity, as well as linearly dependent on the wave frequency. Selecting a wave frequency, the dimensionalized force RAO can be approximated by the following equation:

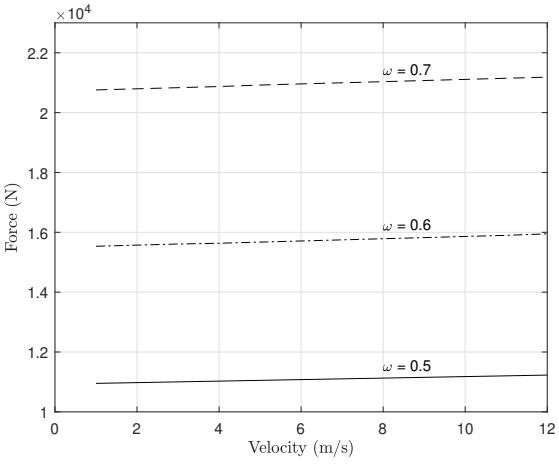

Fig. 1. Surge RAOs at various wave frequencies and surge velocities. The plot is dimensionlized with ρ and g

$$\rho g|F^{\nu}(\nu(t))| \approx a\nu(t) + b, \tag{7}$$

where $a = 23.18$, $b = 10845$, for the wave frequency, ω, of 0.5 rad/s. Note, the force RAO magnitude, $|F^{\nu}(\nu(t))|$, typically uses a subscript to indicate first order wave forces or second order drift forces. This paper only discusses first order wave forces so the subscript is excluded.

Wave Environment The force imparted on the boat from the wave is dependent upon the wave height and boat position. For a single harmonic in the surge direction the wave elevation is defined as:

$$\xi(\chi_{\mathrm{e}}, t) = a_h \cos(k\chi_{\mathrm{e}} - \omega t + \epsilon), \tag{8}$$

where a_h is the wave amplitude, ϵ is an arbitrary added phase, and $\chi_{\mathrm{e}} \in \mathbb{R}$ is the boat's position in an inertial reference frame. Assuming the boat's χ-axis coincides with the fixed reference frame χ_{e}-axis, χ_{e} can be described in the boat's body fixed frame by (Pérez and Blanke, 2002):

$$\chi_{\mathrm{e}} = \chi_0 + \int \nu(t)\, dt. \tag{9}$$

Inserting (9) into (8) and setting $\chi_0 = 0$ results in the wave elevation described in the boat's reference frame:

$$\xi(\chi, t) = a_h \cos\left(\int \nu(t)\, dt - \omega t - \epsilon\right). \tag{10}$$

With the deep water dispersion relation $k = \omega^2/g$ is assumed, the wave force term in (1b) is a function of the force RAO (7) and the wave elevation (10):

$$\tau_{\mathrm{w}}^{\nu}(\nu(t), \eta(t)) = -\rho g|F^{\nu}(\nu(t))|a_h \cos\left(\omega t + \frac{\omega^2}{g}\int \nu(t)\, dt + \phi_{\mathrm{RAO}} + \epsilon\right), \tag{11}$$

where g is the acceleration due to gravity, $|F^{\nu}(\nu(t))|$ is the force RAO, and ϕ_{RAO} is the phase RAO which is assumed

constant at 1.502 radians. Note, typical notation for the wave frequency ω, wave amplitude a_h, and ϵ include a k subscript to indicate each wave component, however, to avoid confusion with the discrete time indices later, and since this paper only concerns a single wave component, the subscript has been dropped.

Next, the wave harmonic is decoupled from the height and force RAO to simplify use in state space form and is redefined as:

$$\eta(t) := \cos\left(\omega t + \frac{\omega^2}{g}\int \nu(t)\,dt + \phi_{\text{RAO}} + \epsilon\right). \tag{12}$$

The dynamics of $\eta(t)$ are obtained by differentiating (12) with respect to time. The resulting expressions are somewhat involved, but can be simplified significantly by performing an order of magnitude analysis to retain only the leading-order terms under the following set of assumptions:

- $\omega \in [0.30, 0.75]$ rad/s. This is justified by observing that the vast majority of wave energy in a typical wave energy spectrum is concentrated in this band.
- $\nu(t) \in [0, 10]$ m/s. This is the typical operating range in surge velocity for the ASV studied.
- $\frac{\omega^2}{g}\dot{\nu}(t) \ll \omega + \frac{\omega^2}{g}\nu(t)$ so it is neglected.

With these assumptions the first derivative is:

$$\dot{\eta}(t) \approx -\left(\omega + \frac{\omega^2}{g}\nu(t)\right)\sin\left(\omega t + \frac{\omega^2}{g}\int \nu(t)dt + \phi_{\text{RAO}} + \epsilon\right). \tag{13}$$

The second derivative is:

$$\ddot{\eta}(t) \approx -\left(\omega + \frac{\omega^2}{g}\nu(t)\right)^2 \eta(t). \tag{14}$$

The term $\omega + \frac{\omega^2}{g}\nu(t)$ is the encounter frequency of the boat to a wave in a head sea.

2.3 Combined State Space Model

The combined surge and wave dynamics can be expressed in linear time varying form as shown in (Tomás-Rodríguez and Banks, 2010). Here, in (15), it is clear to see the coupling between the boat velocity and the wave state. The force of the wave imparted on the boat in the (2,4) term is dependent on both the velocity of the boat and the wave state, while in the (5,4) term, the square of the encounter frequency can be seen. Linearization of this system about a fixed velocity loses this coupling. This motivates the use of a nonlinear control technique.

3. CONTROLLER DESIGN

The following section presents the design of a Nonlinear Model Predictive Controller based on a condensed single-shooting approach. The optimisation is implemented within the Real Time Iteration Scheme (RTI) (Diehl et al., 2005) which is a popular method to achieve real-time performance.

3.1 NMPC Controller

Considering a discrete-time representation of the general nonlinear system (15), the objective is to minimize a cost function of the form,

$$J = (Y_r - \hat{Y})^T Q (Y_r - \hat{Y}) + (U_r - \hat{U})^T R (U_r - \hat{U}) \tag{16a}$$

$$s.t.$$

$$x_k = x_0 \tag{16b}$$

$$x_{k+1} = f(x_k, u_k), \tag{16c}$$

$$y_k = g(x_k, u_k), \tag{16d}$$

$$U_{min} \le \hat{U} \le U_{max} \tag{16e}$$

$$Y_{min} \le \hat{Y} \le Y_{max} \tag{16f}$$

where $x_k \in \mathbb{R}^{n_x}$ are the states of the system at time k, $u_k \in \mathbb{R}^{n_u}$ are the inputs, and $y_k \in \mathbb{R}^{n_y}$ are the outputs. Moreover, $Q > 0 \in \mathbb{R}^{N_p n_y \times N_p n_y}$ and $R > 0 \in \mathbb{R}^{N_p n_u \times N_p n_u}$ are positive definite matrices for penalizing output and input errors, respectively; $Y_r, \hat{Y}, U_r, \hat{U}$ are column-vectors containing future output references, output predictions, input references and input predictions, respectively; and the optimisation subject to initial condition (16b), state dynamics (16c), state-output function (16d), and input and output constraints (16e) and (16f).

Cost function (16) is a Nonlinear Programming Problem (NLP), which is in general difficult to solve. Popular alternatives are Sequential Quadratic Programming (SQP) methods which form a linearized Convex Quadratic Program to find an optimal search direction which eventually drives the solution towards a local optimum. In predictive control, the linearization of the cost function is only defined after the future inputs and states trajectories are defined. To address this, single-shooting methods use an initially guessed nominal input trajectory $\bar{U} = [\bar{u}_k^T, \bar{u}_{k+1}^T, \cdots, \bar{u}_{k+N_p-1}^T]^T$ which can be used to obtain the nominal state and output trajectories, $\bar{X} = [\bar{x}_{k+1}^T, \bar{x}_{k+2}^T, \cdots, \bar{x}_{k+N_p}^T]^T$ and $\bar{Y} = [\bar{y}_{k+1}^Y, \bar{y}_{k+2}^T, \cdots, \bar{y}_{k+N_p}^T]^T$, respectively, by propagating the input through the state dynamics (16c) and obtaining the respective outputs through output function (16d).

By taking a first order Taylor approximation, with a slight abuse of notation, all future inputs and outputs can then be obtained starting from an initial condition mismatch δx_0 related to the Real-Time Iteration Scheme as,

$$\hat{U} = \bar{U} + \delta\hat{U} \tag{17a}$$

$$\hat{Y} = \bar{Y} + \delta\hat{Y} = \bar{Y} + G\delta x_0 + F\delta\hat{U} \tag{17b}$$

where matrices G and F are defined as

$$\begin{bmatrix} \dot{\chi}(t) \\ \dot{\nu}(t) \\ \dot{\zeta}(t) \\ \dot{\eta}_k(t) \\ \ddot{\eta}_k(t) \end{bmatrix} = \begin{bmatrix} 0 & 1 & 0 & 0 & 0 \\ 0 & -\frac{D(\nu(t))}{M} & \frac{\tau_{\text{p}}(\nu(t),\zeta(t))}{M} & -\frac{\rho g |F^u(\nu(t))| a_h}{M} & 0 \\ 0 & 0 & -\frac{1}{\kappa} & 0 & 0 \\ 0 & 0 & 0 & 0 & 1 \\ 0 & 0 & 0 & -\left(\omega + \frac{\omega^2}{g}\nu(t)\right)^2 & 0 \end{bmatrix} \begin{bmatrix} \chi(t) \\ \nu(t) \\ \zeta(t) \\ \eta_k(t) \\ \dot{\eta}_k(t) \end{bmatrix} + \begin{bmatrix} 0 \\ 0 \\ \frac{1}{\kappa} \\ 0 \\ 0 \end{bmatrix} u(t) \tag{15}$$

$$G = \begin{bmatrix} C_1A_0 \\ C_2A_1A_0 \\ \vdots \\ C_{N_p}A_{N_p-1}\cdots A_1A_0 \end{bmatrix}, \tag{18a}$$

$$F = \begin{bmatrix} C_1B_0 & \mathbb{0} & \cdots & \cdots \\ C_2A_1B_0 & C_2B_1 & \mathbb{0} & \cdots \\ C_3A_2A_1B_0 & C_3A_2B_1 & C_3B_2 & \cdots \\ \vdots & \vdots & \vdots & \ddots \\ C_{N_p}A_{N_p-1}\cdots A_1B_0 & C_{N_p}A_{N_p-2}\cdots A_2B_1 & \cdots & \cdots \end{bmatrix}. \tag{18b}$$

and,

$$A_k = \left.\frac{\partial f(\hat{x}_k,\hat{u}_k)}{\partial \hat{x}_k}\right|_{\substack{\hat{x}_k=\bar{x}_k \\ \hat{u}_k=\bar{u}_k}} B_k = \left.\frac{\partial f(\hat{x}_k,\hat{u}_k)}{\partial \hat{u}_k}\right|_{\substack{\hat{x}_k=\bar{x}_k \\ \hat{u}_k=\bar{u}_k}} \tag{19a}$$

Moreover, this paper focuses on regulating the average boat velocity and minimizing the wave forces defined as:

$$\tau_{\mathrm{w}} = \bar{\tau}_{\mathrm{w}} + \frac{\partial \tau_{\mathrm{w}}(\bar{\nu}_k,\bar{\eta}_k)}{\partial \nu_k}\delta\nu_k + \frac{\partial \tau_{\mathrm{w}}(\bar{\nu}_k,\bar{\eta}_k)}{\partial \eta_k}\delta\eta_k. \tag{20}$$

thus, resulting in the output matrix defined as:

$$C_i = \begin{bmatrix} 0 & 1 & 0 & 0 \\ 0 & \frac{\partial \tau_{\mathrm{w}}(\bar{u}_k,\bar{\eta}_k)}{\partial \nu_k} & 0 & \frac{\partial \tau_{\mathrm{w}}(u_k,\eta_k)}{\partial \eta_k} \end{bmatrix}. \tag{21}$$

The wave force in the surge direction does not vary by a large amount with a change in velocity which can be seen in Figure 1. Using an additional tuning parameter in the force RAO equation, (7) can be rewritten as:

$$|F_k^{\nu}(\nu_k)| = \alpha(a\nu_k) + b, \tag{22}$$

where α is the additional tuning weight which can be used to virtually increase the change in the wave force with respect to the boat velocity.

To obtain a desired average velocity, the rows of the linearized prediction model (17b) related to the velocity are averaged over the prediction horizon.

Optimization Substituting input and output linearised prediction models (17a) and (17b) in the original cost function (16), and rearranging the cost in terms of the decision variable $\delta\hat{U}$ (condensing approach) results in the standard QP form:

$$J = \frac{1}{2}\delta\hat{U}^T H\delta\hat{U} + \delta\hat{U}^T f + C \tag{23a}$$

s.t.

$$M\delta\hat{U} \leq \gamma \tag{23b}$$

$$H = F^T QF + R \tag{23c}$$

$$f = -\left[F^T Q(Y_r - \bar{Y} - G\delta x_0) - R(\bar{U} - U_r)\right] \tag{23d}$$

$$M = \begin{bmatrix} I \\ -I \\ F \\ -F \end{bmatrix} \quad \gamma = \begin{bmatrix} U_{max} - \bar{U} \\ -(U_{min} - \bar{U}) \\ Y_{max} - \bar{Y} - G\delta x_0 \\ -(Y_{min} - \bar{Y} - G\delta x_0) \end{bmatrix} \tag{23e}$$

Having defined this, any QP solver of choice can be used to solve (23a). Once the optimal input deviation, $\delta\hat{U}$, is obtained, equation (17a) is used to recover the actual input. Only the first input is applied to the system, and the process is then repeated, which is the well known receding horizon strategy.

3.2 Real Time Iteration Scheme

The Real Time Iteration (RTI) scheme, is a strategy that enables real-time performance for Nonlinear Optimal Control. The following is a brief explanation of the procedure.

Initial Value Embedding (IVE) It uses the solution found in the previous step in a shifted version, typically duplicating the last input variable $u_{k+N_p|k+1} = u_{k+N_p-1|k}$, to obtain the nominal trajectory over which the formulation will linearise and optimise.

Single SQP To further reduce the computational burden and achieve predictable timings, only a single step of the SQP is performed. This is reasonable given that the solution is "hot-started" from the previous solution, which is expected to be close to the optimal solution, provided no significant unknown/unexpected disturbances have entered the system.

Computation Separation Separates the computations into preparation and feedback phases to avoid the computation delay related to the preparation of the QP. Diagrams showing the timings of these phases can be found in Gros et al. (2016).

(1) Preparation Phase: In between sampling times, the preparation phase uses a predicted nominal state for the next sampling time $\bar{x}_0 = \hat{x}_{k|k-1}$ as a starting point obtained from the last state $x_{k-1|k-1}$ and last input $u_{k-1|k-1}$ which allows the preparation of the QP main matrices $H, M, F, etc.$, and partially, vectors f and γ.
(2) Feedback Phase: Once the current state measurement becomes available the feedback phase calculates the state mismatch $\delta x_0 = x_0 - \bar{x}_0$, finishes the calculation of f and γ, and solves the QP. In some cases, it may be beneficial to run the QP prior to the state measurement assuming $\delta x_0 = 0$ to obtain an estimate of the Lagrange multipliers, λ, related to the inequalities constraints. In this strategy, the optimal solution obtained from the RTI can be shown to have the form as presented in Wang (2011):

$$\hat{U} = \bar{U} - H^{-1}\left[\underbrace{\overbrace{-(F^TQ(Y_r-\bar{Y}) - R\bar{U})}^{\text{Unconstrained}}\ \overbrace{+M^T\lambda}^{\text{Constrained}}}_{\text{Preparation Phase}}\ \underbrace{+F^TQG\delta x_0}_{\text{Feedback Phase}}\right] \tag{24}$$

4. SIMULATION RESULTS

The boat was simulated heading directly into oncoming waves with the propellers being the only actuation. The wave was a single harmonic with a wave height of 1 meter and a frequency of 0.5 rad/s. The NMPC had a prediction horizon of 200 steps ahead, with the sample period 0.08 seconds resulting in a prediction window of 16 seconds which captures just over one complete harmonic. The simulation was run for 30 seconds. The weights of the NMPC were $Q_u = 10$ for penalizing deviations of the average velocity from the desired average, $R_u = 1.4 \times 10^{-7}$ penalizing deviations from U_r, and the tuning weight in (22) is set as $\alpha = 100$. The following shows a comparison

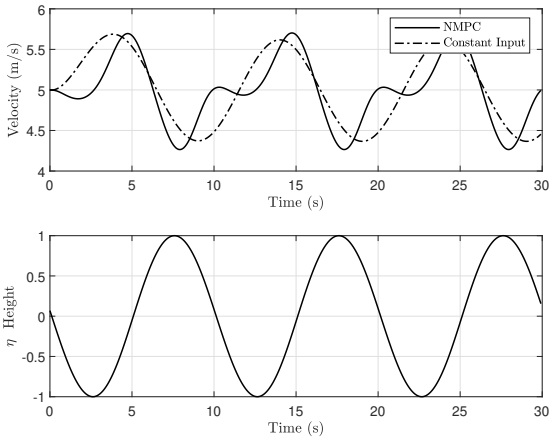

Fig. 2. The top plot shows the velocity profiles of the two controllers. The bottom plot shows the wave state η. The velocity profile shows a global minimum for the NMPC controlled boat when η is maximum and a local minimum when η is minimum.

between a constant propeller input which produces an average 5 m/s velocity and the NMPC controller with a desired average velocity of 5 m/s.

Figure 2 shows the velocity profiles of the open loop controller and the NMPC controller compared to the wave state, η. A clear difference in the velocity profiles can be seen. The open loop controller has an oscillating, single harmonic velocity resulting from changes only in the wave force, while the NMPC scenario has a more complex velocity profile. A global minimum of velocity for the NMPC controller occurs when the wave state is at its maximum, while a local minimum velocity for the NMPC controller occurs at the minimum of the wave state. Both the local and global maximum velocity occurs when the wave state is at zero. This behavior allows the boat to maintain the desired average velocity while reducing peak wave forces.

The resulting force on the boat can be seen in Figure 3. This figure shows the weighted wave force as calculated from (22). The base force, that which the boat would experience at 0 m/s, is subtracted from this figure to better show the difference in the two scenarios. Figure 4 shows the input for both controllers as it compares to the wave state. The NMPC input frequency appears to be twice that of the wave. This double harmonic is confirmed when looking at Figure 5. This figure shows the amplitude spectrum of the input signal to the propeller for NMPC. In the simulation, with an average velocity of 5 m/s the average encounter frequency of the boat is 0.628 rad/s, which has a small peak in the amplitude spectrum, while a much larger peak in seen at 1.256 rad/s or double the average encounter frequency. This can be explained by the fact that for each wave period, the minimal wave force occurs twice. NMPC exploits this by having the velocity profile shown in Figure 2, with peaks during the minimal wave force time.

5. CONCLUSION AND FUTURE WORK

This paper formulated and solved the problem of minimizing wave-induced forces upon an ASV heading into

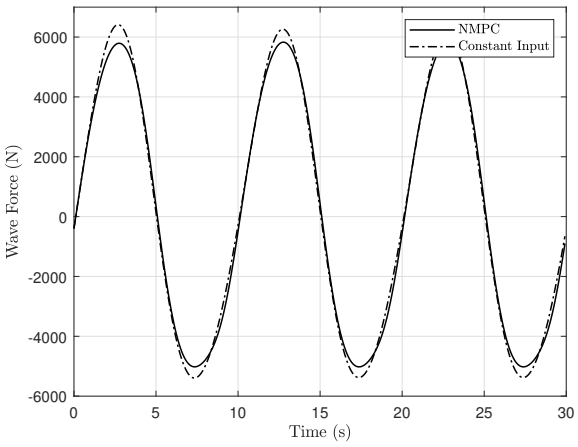

Fig. 3. Wave force comparison between the two controllers. Note: The base wave force is subtracted to more clearly show the difference in the two controllers.

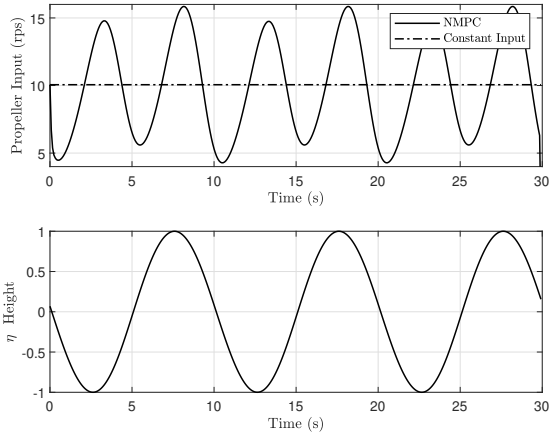

Fig. 4. The top plot shows the propeller input profiles of the two controllers. The bottom plot shows the wave state η.

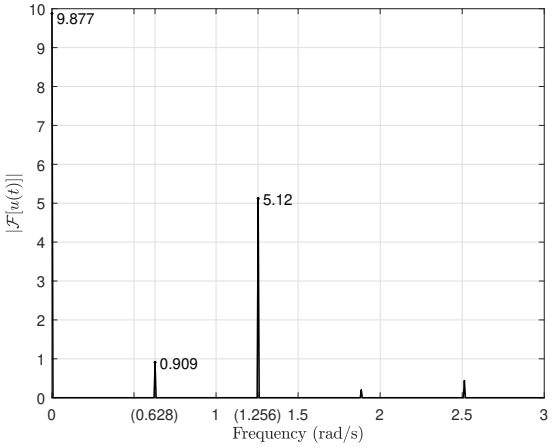

Fig. 5. An amplitude spectrum of the NMPC controller input

ocean waves. Because of the velocity-dependent encounter frequency, linearization of the dynamics removes the important coupling between the vessel and the wave, hence motivating the use of a NMPC which can benefit both, from the future prediction of the wave, as well as the ability to handle nonlinear dynamics and constraints. Moreover, a key finding of this study was observed in the velocity and input profiles required to minimize wave forces which resulted in twice the average encounter frequency. Further studies will seek to use this coupling concept to explore other degrees of freedom such as pitch and roll as well as the additional input of steering, and use NMPC's ability to reduce forces and satisfy constraints to handle more complex sea states.

REFERENCES

Çimen, T. and Banks, S.P. (2004). Nonlinear optimal tracking control with application to super-tankers for autopilot design. *Automatica*, 40(11), 1845–1863.

Diehl, M., Bock, H.G., and Oder, J.P.S. (2005). A real-time iteration scheme for nonlinear optimization in optimal feedback control. 43(5), 1714–1736.

Fossen, T.I. (2011). *Handbook of marine craft hydrodynamics and motion control*. John Wiley & Sons.

Gros, S., Zanon, M., Quirynen, R., and Bemporad, A. (2016). From linear to nonlinear MPC : bridging the gap via the real-time iteration. 7179.

Heins, P.H., Jones, B.L., and Taunton, D.J. (2017). Design and validation of an unmanned surface vehicle simulation model. *Applied Mathematical Modelling*, 48, 749–774.

Kim, Y.H., Lee, S.W., Yang, H.S., and Shell, D.A. (2012). Toward autonomous robotic containment booms: Visual servoing for robust inter-vehicle docking of surface vehicles. *Intelligent Service Robotics*, 5(1), 1–18.

Lekkas, A.M. and Fossen, T.I. (2014). Minimization of cross-track and along-track errors for path tracking of marine underactuated vehicles. In *2014 European Control Conference, ECC 2014*.

Li, Z., Sun, J., and Oh, S. (2009). Path following for marine surface vessels with rudder and roll constraints: An MPC approach. *Proceedings of the American Control Conference*, 3611–3616.

Li, Z., Sun, J., and Oh, S. (2010). Handling roll constraints for path following of marine surface vessels using coordinated rudder and propulsion control. *Proceedings of the 2010 American Control Conference*, 6010–6015.

Merigaud, A. and Ringwood, J.V. (2019). Incorporating Ocean Wave Spectrum Information in Short-Term Free-Surface Elevation Forecasting. *IEEE Journal of Oceanic Engineering*, 44(2), 401–414.

Oh, S.R. and Sun, J. (2010). Path following of underactuated marine surface vessels using line of sight based model predictive control. *Ocean Engineering*, 37(2-3), 289–295.

Oleynikova, E., Lee, N.B., Barry, A.J., Holler, J., and Barrett, D. (2010). Perimeter patrol on autonomous surface vehicles using marine radar. *OCEANS'10 IEEE Sydney, OCEANSSYD 2010*, 1–5.

Ono, M., Quadrelli, M., and Huntsberger, T.L. (2014). Safe maritime autonomous path planning in a high sea state. In *Proceedings of the American Control Conference*, 4727–4734.

Paliotta, C., Lefeber, E., Pettersen, K.Y., Pinto, J., Costa, M., and De Figueiredo Borges De Sousa, J.T. (2019). Trajectory Tracking and Path following for Underactuated Marine Vehicles. *IEEE Transactions on Control Systems Technology*, 27(4), 1423–1437.

Pérez, T. and Blanke, M. (2002). Simulation of Ship Motion in Seaway. 1–13.

Peymani, E. and Fossen, T.I. (2013). 2D path following for marine craft: A least-square approach. In *IFAC Proceedings Volumes (IFAC-PapersOnline)*, volume 9, 98–103. Toulouse, France.

Reinhart, R.F., Steil, J.J., Huntsberger, T.L., and Stoica, A. (2010). Tacking reduces bow-diving of high-speed Unmanned Sea Surface Vehicles. In *Proceedings - EST 2010 - 2010 International Conference on Emerging Security Technologies, ROBOSEC 2010 - Robots and Security, LAB-RS 2010 - Learning and Adaptive Behavior in Robotic Systems*, 177–182.

Tomás-Rodríguez, M. and Banks, S.P. (2010). *Linear, time-varying approximations to nonlinear dynamical systems: With applications in control and optimization*, volume 400. Springer Verlag.

Wang, L. (2011). *Model Predictive Control System Design and Implementation Using MATLAB*. Springer.

Appendix A. MODEL PARAMETERS

Table A.1. Halcyon Parameters

Name	Symbol	Value
Mass	M	11000 kg
Max Surge Velocity	$\nu^{\max}$	10 m/s
Propeller Diameter	d	0.622 m
Propeller Time Constant	κ	1.8 s
Wetted Surface Area	S	36.36 m^2
Water Density	ρ	1025 kg/m^3
Wave Amplitude	a_h	1 m
Wave Frequency	ω	0.5 rad/s
Acceleration due to Gravity	g	9.81 m/s^2
Phase RAO	ϕ_{RAO}	1.502 radians
Force RAO Slope	a	23.18 N/(m/s)
Force RAO Intercept	b	10845 N
RAO Tuning Weight	α	100

Table A.2. p Constant Coefficients

p_1	-9.22×10^{-7}	p_5	-5.52×10^{-3}
p_2	3.14×10^{-5}	p_6	2.49×10^{-3}
p_3	-4.00×10^{-4}	p_7	1.70×10^{-2}
p_4	2.31×10^{-3}		

Table A.3. $K_\tau^{\{i\}}$ Thrust Polynomial Constants

$K_\tau^{\{1\}}$	0.0041
$K_\tau^{\{2\}}$	-0.5002
$K_\tau^{\{3\}}$	0.6008